Si nanoparticles as sensitizers for radio frequency-induced cancer hyperthermia

A. V. Kabashin[*a], K. P. Tamarov[b], Yu.V. Ryabchikov[a,c], L. A. Osminkina[b,d], S. V. Zinovyev[e], J. V. Kargina[b], M. B. Gongalsky[b,d], A. Al-Kattan[a], V. G. Yakunin[b], M. Sentis[a], A. V. Ivanov[e], V. N. Nikiforov[b], A. P. Kanavin[c,d], I. N. Zavestovskaya[c,d], V. Yu. Timoshenko[†b,c,d]

[a]LP3, Aix-Marseille University, UMR CNRS 7341, Campus de Luminy , Case 917, 13288, Marseille Cedex 9, France; [b]Physics Department, Moscow State M. V. Lomonosov University, 119992 Moscow, Russia; [c]Lebedev Physical Institute of Russian Academy of Sciences, 53 Leninskii Prospekt, Moscow 199 991, Russia; [d]National Research Nuclear University "MEPhI" (Moscow Engineering Physics Institute), International Laboratory "Bionanophotonics", 115409 Moscow, Russia, [e]Russian Cancer Research Blokhin Center, 115478 Moscow, Russia,

ABSTRACT

We review our recently obtained data on the employment of Si nanoparticles as sensitizers of radiofrequency (RF) - induced hyperthermia for mild cancer therapy tasks. Such an approach makes possible the heating of aqueous suspensions of Si nanoparticles by tens of degrees Celsius under relatively low intensities (1–5 W/cm^2) of 27 MHz RF radiation. The heating effect is demonstrated for nanoparticles synthesized by laser ablation in water and mechanical grinding of porous silicon, while laser-ablated nanoparticles demonstrate a remarkably higher heating rate than porous silicon-based ones for the whole range of the used concentrations. The observed RF heating effect can be explained in the frame of a model considering the polarization of Si NPs and electrolyte in the external oscillating electromagnetic field and the corresponding release of heat by electric currents around the nanoparticles. Our tests evidence relative safety of Si nanostructures and their efficient dissolution in physiological solutions, suggesting potential clearance of nanoparticles from a living organism without any side effects. Profiting from Si nanoparticle-based heating, we finally demonstrate an efficient treatment of Lewis Lung carcinoma *in vivo*. The obtained data promise a breakthrough in the development of mild, non-invasive methods for cancer therapy.

Keywords: silicon nanoparticles, RF-heating, laser ablation, biological application

1. INTRODUCTION

The ability of radio frequency (RF) radiation to heat human tissues is known for a long time. In particular, such a heating of malignant tissues can lead to a successful partial necrosis of tumors giving a promise for successful application of RF radiation in cancer treatment tasks [1-3]. However, in the absence of vectoring mechanism to selectively target tumors, RF radiation-based therapy appears to be dangerous as the improvement of blood circulation under RF irradiation can provoke a further development of tumors and their metastasis [3].

The efficiency of RF-based therapy can be significantly enhanced by using sensitizers, or properly designed absorbing agents, which are targeted into a tumor area (actively or passively), accumulate in it, and then absorb main RF radiation power to heat cancer cells and thus cause their selective destruction. Such an effect can be achieved by using electrically-

[*]kabashin@lp3.univ-mrs.fr (+33) 491829383;
[†]timoshen@physics.msu.ru (+7) 9163789811

Synthesis and Photonics of Nanoscale Materials XIII, edited by
Andrei V. Kabashin, David B. Geohegan, Jan J. Dubowski, Proc. of SPIE
Vol. 9737, 97370A · © 2016 SPIE · CCC code: 0277-786X/16/$18 · doi: 10.1117/12.2222814

conductive nanoparticles (NPs) [4-7]. Gold nanoparticles and carbon nanotubes were selected as candidates for these tasks providing a strong absorption of RF radiation even under relatively small concentrations of NPs of the order of 1 g/l [5-7]. In particular, an intense source of the RF radiation with frequency of 13.6 MHz and the power of 600 W induced heating of suspensions of gold (Au) NPs with heating rate ~20 K/sec, which resulted in considerable cell necrosis [7]. As we recently showed, similar hyperthermia effect can be achieved for weakly conductive Si nanostructures [8]. Although a strong heating of Si nanoparticles is not explained in terms of theories based on conductive properties of nanostructures [5], the heating effect was significant and even more pronounced than in the case of Au nanoparticles. In particular, we were able to heat suspensions of Si nanoparticles at relatively low concentrations (below 1 mg/mL) to temperatures above 45-50^{o} C applying relatively low 27 MHz radiation intensities (1-5 W/cm^2). We believe that Si nanoparticles can present a much more promising object as a RF radiation sensitizer compared to other inorganic nanomaterials. First, Si NPs are biocompatible and biodegradable, as in biological tissue they normally decay into orthosilicic acid $Si(OH)_4$, which is naturally excreted from the body through the urine [9]. In addition, Si nanoparticles can be prepared in pure, uncontaminated state by e.g. using methods of laser ablation in gaseous [10-13] or aqueous [14-18] ambience, which excludes any secondary biotoxicity related to the contamination of the nanoparticle surface. Finally, Si nanoparticles can exhibit a series of unique properties, including room temperature photoluminescence [19,20], singlet oxygen generation under photoexcitation [21,22], infrared radiation–induced [23] and ultrasound-induced [24] hyperthermia, which can be applied in parallel to the RF hyperthermia approach.

In this paper, we review recently obtained results on properties and conditions of employment of Si nanoparticles as sensitizers of radio-frequency-based hyperthermia.

2. EXPERIMENTAL METHODS

2.1 Fabrication and characterization of Si nanoparticles

First, we formed porous Si (por-Si) films by electrochemical etching (anodization) of heavily boron-doped crystalline silicon (c-Si) wafers with specific resistivity of 1-10 *mΩ·cm* in HF (48%):C_2H_5OH solution (1:1) at the current density of 60 *mA/cm*^{2} and etching time of 60 *min*. The por-Si films were separated from c-Si substrates by applying a pulse of the etching current with current density of 600 *mA/cm*^{2}. The as-prepared Por-Si consisted of 5-10 *nm*-sized Si nanocrystals and pores with diameter above 2 nm (mesopores). The porosity of as-prepared samples was about 70 ± 5%, as determined by gravimetric methods. The porous silicon films were then milled in distilled deionized water by using a planetary mill FRITSCH "Pulverisette 7 premium line" and then centrifuged in an Eppendorf Centrifuge 5424 for 1 min at 2000 rpm. Second, we used methods of ultrashort laser ablation to fabricate ultrapure Si-based nanoparticles [16,17]. Briefly, a Si target was placed at the bottom of a glass vessel filled with 20 ml of highly deionized water (18.2 MΩcm). A 2.3 mm diameter beam of Yb:KGW femtosecond laser (Amplitude Systems [Pessac, France], 1025 nm, 480 fs, 500 μJ, 1–5 kHz) was focused with the help of a 750 mm lens onto the target surface to provide ablation of material [14,15]. The target was moved at a scanning velocity of 0.35 mm/s in the focusing plane to obtain identical surface conditions during the laser ablation, while the thickness of the water layer above the target was about 1 cm. Such ablation geometry normally leads to a grey coloration of the aqueous solution after 2–5 minutes of the experiment. As the second protocol, we employed methods of two step femtosecond laser fragmentation procedure introduced in our previous studies [15,25]. The 10 ml of NPs solution prepared by the first protocol was transferred into a glass cuvette and irradiated, in the very center of the cuvette, by a focused laser beam of the Yb:KGW femtosecond laser (using the same focusing lens), while the solution was stirred by a magnet to homogenize the ablation process. We used relatively low laser fluence (1 J/cm^2) to avoid the phenomenon of laser-assisted plasma breakdown of the liquid, but the radiation intensity was high enough to ablate the suspended nanoparticles.

The size of Si NPs was determined by using a transmission electron microscope (TEM) LEO912 AB OMEGA. The composition of surface coating of por-Si NPs was studied with a Fourier-transform infrared (FTIR) spectrometer Bruker IFS 66v/S. Before measuring the FTIR spectra, the suspensions of Si NPs were deposited on an ATR crystal and then they were dried in air and evacuated at 10^{-3}Torr.

2.2. Methodology of RF experiments

The RF heating was achieved by applying a medical apparatus, which is commonly used for the RF physiotherapy, with frequency of 27 MHz and maximal power up to 66 W. The apparatus consisted of a power source coupled to a pair of

flat electrodes with diameter of 38 mm and varied distance between them. The RF electrical field strength between the electrodes was measured by using a metallic antenna connected to an oscilloscope Agilent 54642A. The RF radiation intensity calculated from the electric field strength was in good agreement with the RF power per the electrode surface area. Temperatures of aqueous suspensions of Si NPs and pure water (for comparison) were measured using an infra-red thermometer AND DT-633 after switching off the RF generator. To investigate the RF heating process a 20 ml glass cuvette was filled with the aqueous suspension of NPs and it was centered between the RF electrodes spaced apart by 42 mm, allowing approximately a 6 mm air gap on either side of the cuvette. The maximum concentration of NPs in suspensions was 1 g/l, which was estimated using the gravimetrical method. Then the 1 g/l suspension was diluted with distilled water to obtain different concentrations. Prior to the RF exposure, the initial temperature of each sample was stabilized in a thermostat at 21^0 C. The heating rate was quantified by the value of $S = \Delta T/\Delta t$, where ΔT is temperature increase after the RF exposure for time Δt.

2.3. Methodology of *in vivo* tests

In vivo experiments were carried out with lung carcinoma (3LL) tumors inoculated at the left hind paw of male mice of CBA line. The initial tumor volume before the RF treatment was about 210±30 mm^3. The 0.5 ml aqueous suspensions of por-Si or LA-Si NPs or equal volumes of sterile water were intratumorally injected and the mice were kept for 15-20 min prior to exposure in the RF field. Then the mice were immobilized and irradiated with RF (5 W/cm^2) for 2 minutes. The corresponding reference groups of mice without the RF irradiation were also studied. All the experiments with animals were carried out at animal facilities of the Blokhin Cancer Research Centre (Moscow, Russia) in accordance with the Principles of Laboratory Animal Care (NIH publication No. 85-23, revised in 1985) and the European Convention for the Protection of Vertebrate Animals used for Experimental and Other Scientific Purposes (Strasbourg, 18.III.1986, revised by the amending protocol ETS 170). The use of experimental animals was approved by Scientific and Ethic committees of the Blokhin Cancer Research Centre.

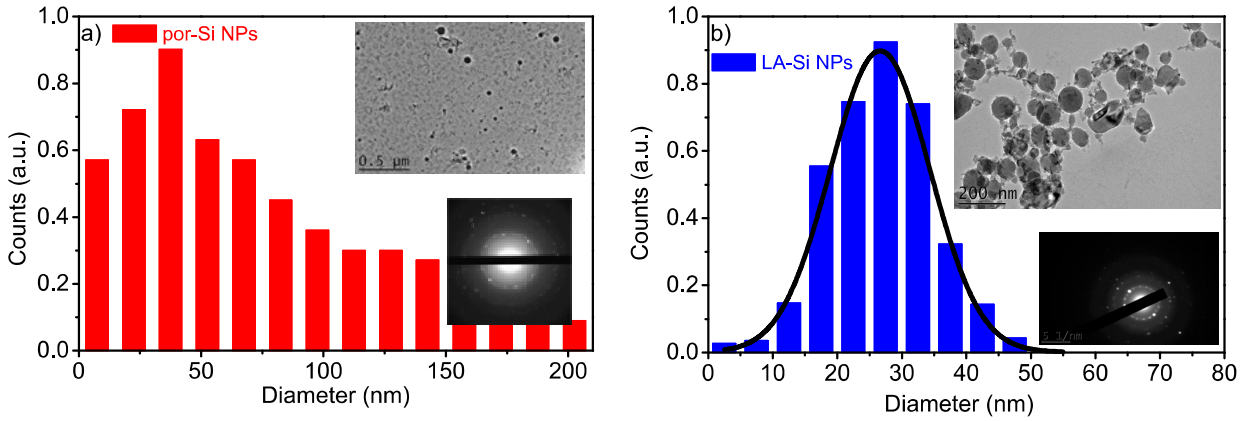

Figure 1. Typical TEM image, Electron Diffraction pattern and size distributions of por-Si NPs (a) and LA-Si NPs (b)

3. RESULTS AND DISCUSSION

3.1 Structural characterization

In this work, we used Si NPs prepared by mechanical milling of porous silicon (Por-Si NPs) and by laser ablation of silicon wafer (LA-Si NPs). An advantage of the first preparation method is fast and cost-efficient production of a large quantity of porous silicon having efficient photoluminescence at room temperature in the visible spectral range. However, a surface of por-Si NPs is contaminated by chemical agents and has to be cleaned properly to remove any residual contaminants. In order to bare NPs without any contamination we have also used a method of fs laser ablation of silicon wafer [14-17]. The main advantage of this method is an absence of any chemical agents and, hence, high purity of nanoparticle surface.

Figure 1 shows size distributions of por-Si NPs (a) and LA-Si (b) NPs, while corresponding TEM images and electron diffraction patterns are shown in figure insets. One can see that por-Si NPs are widely dispersed with mean size around 35 nm. Moreover, a significant part of large NPs (up to 200 nm) is also present. In contrast, LA-Si NPs possess a much narrower size dispersion (less than 15 nm full width at half maximum) with similar value of mean size and nearly spherical NPs shape. A periodic arrangement of reflections is clearly seen in electron diffraction patterns for both types of Si NPs (insets of Figure 1), suggesting crystalline structure of Si NPs. According to our data, the surface of por-Si NPs is predominantly oxidized leading to its hydrophilic properties. Surface of LA-Si NPs is oxidized due to the presence of dissolved oxygen and can be varied by passing neutral gases (e.g., Ar) through the liquid [8,25]. For comparison, we also used Au NPs prepared by fs laser ablation in deionized water (LA-Au NPs) according to the recipe described in [15,25].

3.2 RF radiation-induced heating of Si NPs

ime dependence of the temperature growth of aqueous solutions of por-Si and LA-Si nanoparticles and that of deionized water under RF irradiation (5 W/cm^2) is shown in Figure 2a. It is visible that the heating rate for por-Si NPs is about 10 K/min for NP concentration ~ 1 g/l, which much exceeds that one of deionized water (~ 1 K/min). On the other hand, LA-Si NPs possess 5 K/min heating rate at much lower concentration (~ 0.05 g/l). Here, PSi NPs demonstrated a linear growth of solution temperature under the increase of irradiation time, while for LA-Si NPs the temperature growth rate slightly decreases after some irradiation time (~ 3 min), but still remains relatively high. The reason of this temperature saturation is still not clear, but it can be due to a modification of the surface of LA-Si NPs during RF heating. Concentration dependence of RF heating rate is almost linear for all types of Si NPs (Figure 2b). It is worth noting that heating rate of LA-Si NPs is higher than of por-Si NPs of the same concentration. Thus, por-Si NPs and LA-Si NPs exhibit similar or better heating rate compared to Au NPs, which are widely studied for cancer hyperthermia applications.

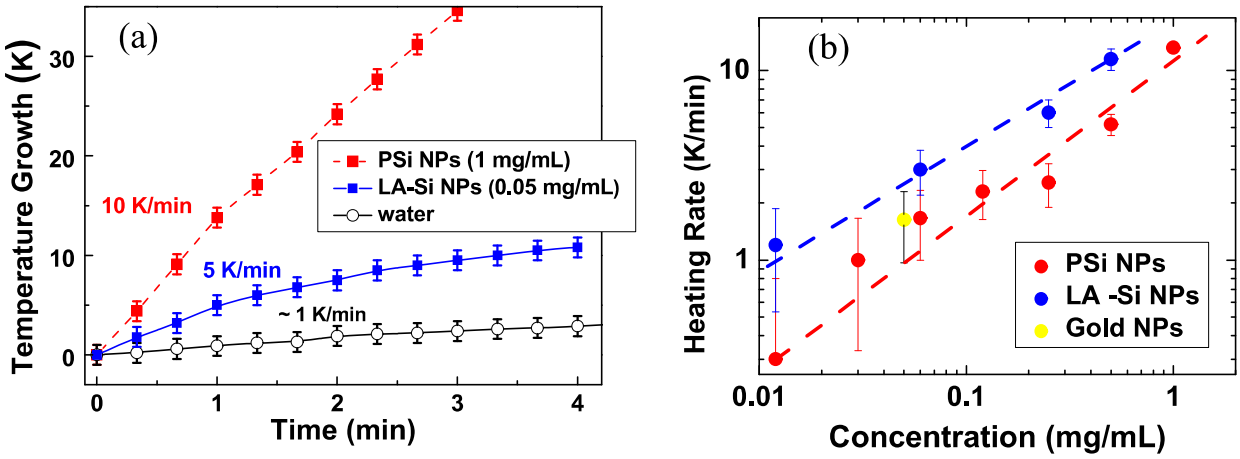

Figure 2. (a) Time dependences of temperature of aqueous suspensions of por-Si NPs (red), LA-Si NPs (blue) and deionized water (black) under RF irradiation; (b) concentration dependence of the heating rate of por-Si NPs (red), LA-Si NPs (blue) and Au NPs (yellow).

3.3 Modeling of RF radiation-induced heating

The obtained results are surprising as they evidence the independence of the RF radiation-induced heating efficiency on electrical conductivity of employed NP-based sensitizers. This conclusion contrasts with widely accepted model of Moran et al. [5], which requires sufficient electrical conductivity of NPs to efficiently absorb RF radiation. According to this model, the Joule heating with rate above 10 *K/min* can be achieved in aqueous suspensions of NPs with concentration of 1 *mg/mL* under RF irradiation with intensity of 1 *W/cm*^{2} if the specific conductivity of NP material is higher than 10^{-1} $\Omega^{-1}cm^{-1}$. However, this situation is not consistent with our case, as such high conductivity is hardly

possible even for Si NPs produced from highly doped crystalline Si wafers [26, 27]. Furthermore, our tests did not reveal any remarkable difference of the temperature growth rates for LA-Si NP suspensions produced from undoped and heavily boron-doped Si wafers. Finally, we did not observe any significant difference in temperature growth rates for low conductive Si and highly conductive Au NPs of similar concentrations (the growth rate of Si NPs was even higher).

In order to explain the observed RF induced heating of NPs we propose a model, which consider main Joule heat sources related to electrical currents of ions in surrounding electrolyte [8]. The ion concentration nearby NPs is supposed to increase because of surface charge (zeta-potential) of NPs or/and their partial dissolution in water. The latter process is obviously more important for Si NPs in comparison with metallic ones. We have carried out simulations of the heating rate by using numerical solution of the Poisson equation and by assuming the Boltzmann statistics for the ion concentration dependent on the electrical potential near randomly distributed non-interacting NPs. The ion production because of the NP dissolution was not taken into account for simplicity. On the one hand, our calculations show a week effect of the heating due to electrical currents inside NPs. On the other hand, gold NPs and Si ones are found to exhibit slightly different heating rates versus the electrolyte conductivity and RF frequency. The modeling allows us to understand the experimentally observed high heating rate of aqueous suspensions of LA-Si NPs under 27 MHz RF irradiation [8]. The model predicts also that the heating contrast between Si NP suspension and homogeneous electrolyte with the same electrical conductivity can be optimized by proper choice of RF frequency. Note the proposed model can be further improved by considering both the effect of NP dissolution and inter-polarization of NPs, which can influence the ion concentration and then the Joule heating rate.

3.4 Dissolubility of Si NPs

The water-solubility and biodegradability of por-Si NPs is well studied in the literature (see e.g., Ref. 9 of the manuscript). In our tests, we examined the solubility of LA-Si NPs in aqueous solutions using TEM and Raman spectroscopy. Aqueous suspensions of LA-Si NPs with initial concentration of 0.5 g/L were diluted with physiological solution (0.9 % NaCl) at the ratio of 1:1. The prepared mixture (1 ml) was put into a dialysis vessel, which was introduced into large amount (5 l) of de-ionized water with fixed pH level of 7.0 at room temperature (20-22 ^{0}C). The experiment was carried out in a dark room to avoid any photoexcitation effects.

The dissolution process was independently studied by Raman spectroscopy under the same dialysis conditions. Droplets containing LA-Si NPs were taken from the solution at different moments after the beginning of the dissolution test, deposited on a metal plate and dried in air. The NPs were then tested by using a micro-Raman spectrometer under excitation with a HeNe laser at 633 nm. As shown in Fig. 3, Raman spectra of the samples exhibited a peak near 520 cm^{-1} associated with the presence of crystalline Si NPs. The position of the peak shifted from 521 cm^{-1} to shorter wavenumbers (519-520 cm^{-1}) after several days of the dissolution process: such a shift is typically attributed to the decrease of the nanoparticle size. In this case, the size of Si nanocrystals can be estimated from the positions of Raman peaks using the well known phonon confinement model. Results of such estimations are shown in an inset of Fig. 3. One can see that the mean size of nanoparticles drops from 30 nm to less than 5 nm a few days after the beginning of the experiment. It should be noted that such Raman spectroscopy cannot precisely follow the size evolution of NPs if they become too small (< 5 nm).

3.5 In vitro toxicity of Si NPs

Hep2 (laryngeal cancer cells) were used for the evaluation of cytotoxicity of PSi and LA-Si NPs. The prepared aqueous suspensions were mixed with DMEM (BioloT, Russia) in the ratio of 1:1, and then the mixtures were added to the cell culture and were incubated for 24 h. The reference cell group was incubated in DMEM. The cell viability was evaluated by using a hemocytometer. Living and dead cells were separated by their coloring with Trypan Blue (Paneco-ltd, Russia). The results were statistically processed using Student's t-test with certainty 0.95. LA-Si NPs demonstrate "zero" toxicity and do not influence Hep2 proliferation for the whole range of NPs concentrations (< 0.06 mg/mL), while Psi NPs demonstrate similar results until very high concentrations (0.6-0.7 mg/mL).

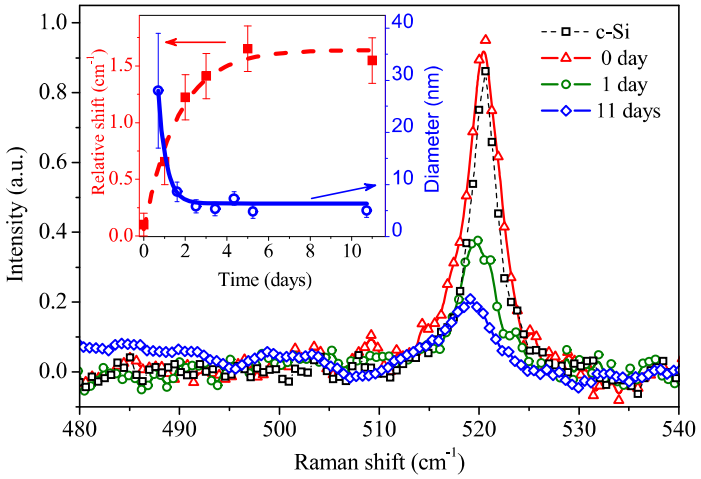

Figure 3. Raman spectra of LA-Si NPs after different times of the storage in water. Relative shift of the Raman spectrum maximum and calculated diameter of NPs are shown in inset.

3.6 In vivo toxicity: effect of Si nanoparticles on the blood content

Wistar rats (male and female) of mass 150±20 g were intragastrically injected with water suspensions of por-Si and LA-Si NPs of dose 0.7 mg/kg. Rats in the control group were similarly injected with distilled water of the same volume. The content of the studied biochemical parameters was determined in blood plasma of experimental animals after a single or sevenfold administration of Si NPs. The animals were sacrificed after 24 hours after the last measurement. The activity of aminotransferase was determined by Reitman-Frankel method (ALT, AST). The activity alkaline phosphatase (ALP) was measured by kinetic method from the increase of coloring of p-nitrophenol in diagnostic kits LaChema (Czech Republic). The cholesterol content was determined by a kinetic method. The concentration of unconjugated and conjugated bilirubin (UB, CB) was determined by Malloy-Evelyn method using VitalDiagnostics kits (Russia) and biochemical analyzer Chem Well (USA). All parameters were compared for the control group and the groups injected with NPs. Statistical analysis of the results was performed using Student's t-test.

The biochemical analysis of blood plasma of the experimental animals injected with por-Si and LA-Si NPs did not reveal any significant changes in the blood content. The intragastric administration (single or seven-fold) of por-Si and LA-Si NPs at the dose of 0.7 mg/kg did not significantly affect the maintenance of transaminase, alkaline phosphatase, bilirubin and cholesterol in blood. The obtained biochemical data were the same for different rat genders. Tables 1 and 2 show the average results of the content of individual cells markers of cytolysis (ATL and AST) during measurement of blood plasma samples. Here, only minor changes of the investigated parameters can be found. Comparing the data of tables 1 and 2, one can notice that a single administration of por-Si NPs induced a slight increase of aminotransferase content in plasma. Although this effect was not significant after sevenfold administration, AST/ALT ratio increased up to 1.5 ± 0.1.

Table 1. Effect of Si NPS on the content of ALT and AST in the rats blood plasma after a single administration

Rat group	ALT, μkat/l	AST, μkat/l	AST/ALT ratio
Control	0.189±0.01	0.231±0.01	1.2±0.1
LA-Si	0.163±0.01*	0.21±0.01*	1.3±0.1*
Psi	0.234±0.01*	0.327±0.02*	1.4±0.1*

*P>0.05

Table 2. Effect of Si NPS on the content of ALT and AST in the rats blood plasma after a sevenfold administration

Rat group	ALT, μkat/l	AST, μkat/l	AST/ALT ratio
Control	0.252±0.01	0.288±0.01	1.1±0.1
LA-Si NPs	0.163±0.01*	0.21±0.01*	1.3±0.1*
Psi	0.174±0.01*	0.271±0.01*	1.5±0.1*

*P>0.05

Table 3. Effect of Si NPS on the content of cholesterol, bilirubin and alkaline phosphatase in the rats blood plasma after a single administration

Rat group	Cholesterol, mmol/l	CB, μmol/l	UB, μmol/l	CB/UB, %	ALP, U/l
Control	1.8±0.1	1.6±0.1	2.2±0.2	73±1.7	484±24
LA-Si NPs	2.0±0.1*	0.7±0.1*	0.8±0.1*	88±1.7*	512±25*
PSi	1.6±0.1*	1.4±0.1*	2.1±0.2*	67±1.6*	529±25*

*P>0.05

Table 4. Effect of Si NPS on the content of cholesterol, bilirubin and alkaline phosphatase in the rats blood plasma after a sevenfold administration

Rat group	Cholesterol, mmol/l	CB, μmol/l	UB, μmol/l	CB/UB, %	ALP, U/l
Control	1.9±0.1	2.5±0.2	2.8±0.2	89±1.8	489±24
LA-Si NPs	1.8±0.1*	0.9±0.1*	1.4±0.1*	64±1.6*	537*±26
PSi	1.7±0.1*	1.0±0.1*	1.3±0.1*	77±1.7*	504*±25

*P>0.05

Table 3 and 4 present data on the content of cholesterol, bilirubin and alkaline phosphatase. One can see that Si NPs did not induce significant changes in cholesterol and bilirubin concentrations after 24 hours after single administration but induced minor reduction after sevenfold administration, while seven-fold administration led to a slight decrease of these parameters. The analysis of plasma samples from groups injected with por-Si and LA-Si NPs also reveals a slight increase in alkaline phosphatase concentration.

In summary, the intragastric administration of aqueous suspensions of por-Si and LA-Si NPs into Wistar rats in dosages 0.7 mg/kg and 4.9 mg/kg does not cause any statistically significant changes in blood levels of aminotrasferases, alkaline phosphatase, bilirubin and cholesterol.

3.7 Results of in vivo RF treatment tests

Fig. 4 shows dependences of the tumor volume for different groups of animals related to the tumor volume of intact mice (sterile water was intratumorally injected). The 0.5 mL aqueous suspensions of Si-based NPs or equal volumes of sterile water were intratumorally injected and the mice were kept for 15-20 min prior to exposure in the RF field. Then the mice were immobilized and irradiated with RF for 2 minutes. Results of the treatment were quantified by the evolution of the total volume occupied by tumor cells. Here, the inhibition of tumor growth was calculated using the following formula:

$$Inhibition = \left(1 - \frac{V}{V_0}\right) \cdot 100\%, \quad (1)$$

where V and V_0 are the averaged tumor volumes for the experimental and reference groups of mice, respectively. The positive value of inhibition indicates the suppression of tumor growth, while the negative one signifies that the average volume for the exposed group of mice was larger than that for the reference group. As shown in Figure 4, a slight

inhibition of the tumor growth takes place under the action of RF radiation alone, which is consistent with previous studies [1-3]. However, our experiments showed that the combined action of PSi NPs and RF excitation can drastically amplify the effect leading to a much stronger inhibition of the tumor growth. Furthermore, as follows from Fig. 4, the efficiency of one time treatment is so high that the average volume of tumor at the 3-rd day after the combined action (V=160 mm^3) becomes smaller than that volume at the very beginning (day 0) of experiment (V_0 = 210 mm^3). In fact, it means that even without any special optimization of the therapy procedure we achieved a partial elimination of the tumor. Here, laser-ablated NPs provides even more pronounced inhibition of tumor growth after the action of RF radiation (V=130 mm^3) and this effect can be observed under much lower number and concentration of NPs (0.2 mL at 0.4 mg/mL compared to 0.5 mL at 1 mg/mL in the case of PSi NPs). Furthermore, we recorded quite different temporal evolution of tumor inhibition after RF treatment using laser-ablated and PSi NPs sensitizers. Here, the maximal tumor inhibition for LA-Si NPs is observed much later (6-7th days compared to the 3rd day for PSi NPs). These data illustrate a different character of the interaction laser-ablated NPs with biological systems.

The obtained results unambiguously show that Si-based nanoparticles can serve as efficient sensitizers for tasks of RF-induced cancer therapy, resulting not only in the inhibition of the tumor growth, but also in its elimination. As shown in Fig. 2c, the efficiency of heating by using Si-based sensitizers appears to be comparable or better than in the case of Au-based NPs. In real cancer treatment procedure, Si-based nanoparticles can be targeted actively, by using proper antibodies, or passively, but profiting from the enhanced permeability and retention (EPR) effect consisting in natural capability of NPs to preferably accumulate in tumors [28]. Here, depending on type of tumor and concrete treatment task, one can select nanoparticles with proper characteristics (size, shape, surface oxidation) and additional functionalities (fluorescence etc). Laser-ablated NPs look especially promising for these tasks as they do not contain any residual contaminant on their surface [17,18], exhibit ideal round shape, controlled mean size and low size-dispersion contributing to their better delivery and uptake *in vivo*.

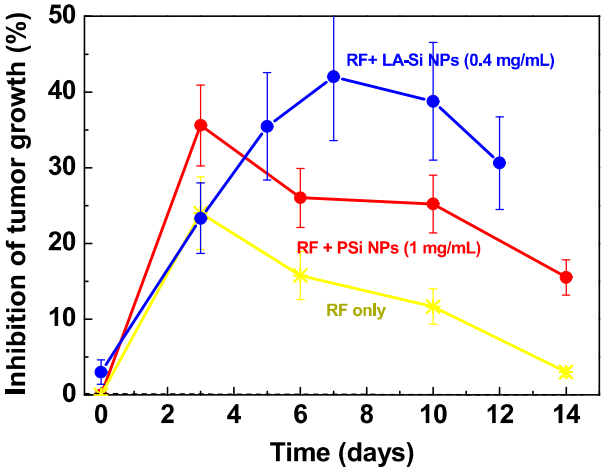

Figure 4. Inhibition of the tumor growth after the following treatments: 2 min treatment of tumor area by RF irradiation with the intensity of 2 W/cm^2 (yellow); injection of por-Si NPs (0.5 mL, 1 mg/mL) followed by 2 min RF irradiation treatment (red); injection of suspension of LA-Si NPs with doses of 0.2 mL and concentration of 0.4 mg/mL followed by 2 min RF irradiation treatment (blue).

4. SUMMARY

We reviewed recently obtained results on the development of novel cancer treatment modalities based on the employment of Si nanoparticles as sensitizers of RF radiation-induced hyperthermia. The hyperthermia effect was observed for Si-based nanoparticles produced by both milling of porous silicon and ultraclean laser-ablative growth and was explained by local currents in the electrical double layer near NP surface. In vivo experiments showed that silicon nanoparticles excited by the RF radiation of relatively low intensity not only strongly inhibited the growth of carcinoma

tumor, but also lead to the decrease of tumor volume. Profiting from potential biodegradability of Si-based nanosensitizers and their prominent optical properties, the proposed RF radiation-based therapy approach looks extremely promising for hyperthermia or/and combined therapy of cancer.

5. ACKNOWLEDGEMENTS

We acknowledge support from the Russian Foundation for Basic Research (grant number 15-52-15041) and France-Russia collaborative PICS 6577 project of DRI CNRS, France. Finally, we acknowledge a support from AMIDEX project (no ANR-11-IDEX-0001-02) funded by the 'Investissements d'Avenir' French Government program, managed by the French National Research Agency (ANR) and by LASERNANOCANCER project of the ITMO "Plan Cancer 2014-2019" of INSERM (No. PC201420).

REFERENCES

[1] Custodio, A., Puente, J., Sastre, J., Diaz-Rubio, E., "Second-line therapy for advanced pancreatic cancer: A review of the literature and future directions," Cancer Treat. Rev. 35, 676–84 (2009).
[2] Mirza, A. N. et al. "Radiofrequency ablation of solid tumors," Cancer J., 7, 95-102 (2001)
[3] Wu, Y. et al., "High operative risk of cool-tip radiofrequency ablation for unresectable pancreatic head cancer," J. Surg. Oncol., 94, 392–5 (2006).
[4] Gannon, C. J. et al., "Carbon nanotube-enhanced thermal destruction of cancer cells in a noninvasive radiofrequency field," Cancer, 110, 2654-2665 (2007).
[5] Moran, C. H. et al., "Size-Dependent Joule Heating of Gold Nanoparticles Using Capacitively Coupled Radiofrequency Fields," Nano Res. 2, 400–405 (2009).
[6] Cherukuri, P.; Glazer, E. S.; Curley, S. A., "Targeted hyperthermia using metal nanoparticles," Adv. Drug Delivery Rev. 62, 339-345 (2010).
[7] Cardinal, J. et al., "Noninvasive radiofrequency ablation of cancer targeted by gold nanoparticles," Surgery 144, 125–132 (2008).
[8] Tamarov, K. P., Osminkina, L. A.; Zinovyev, S. V.; Maximova, K. A.; Kargina, J. V.; Gongalsky, M. B.; Ryabchikov, Yu.; Al-Kattan, A.; Sviridov, A. P.; Sentis, M.; Ivanov, A. V.; Nikiforov, V. N.; Kabashin, A. V.; Timoshenko, V. Yu., "Radio Frequency Radiation-Induced Hyperthermia Using Si Nanoparticle-Based Sensitizers for Mild Cancer Therapy," Sci. Rep., 4, 7034 (2014).
[9] Park, J.-H et al, "Biodegradable Luminescent Porous Silicon Nanoparticles for in Vivo Applications," Nat. Mater., 8, 331–336 (2009).
[10] Umezu, I., Shibata, K., Yamaguchi, S., Sugimura, F., Yamada, Y., Yoshida, T. "Effects of thermal processes on photoluminescence of silicon nanocrystallites prepared by pulsed laser ablation," J. Appl. Phys., 84, 6448-6450 (1998).
[11] Patrone, L., Nelson, D., Safarov, V. I., Sentis, M., Marine, W., Giorgio, S. "Photoluminescence of silicon nanoclusters with reduced size dispersion produced by laser ablation," J. Appl. Phys., 87, 3829-3837 (2000).
[12] Kabashin, A. V., Meunier, M., Leonelli, L., "Photoluminescence characterization of Si-based nanostructured films produced by pulsed laser deposition in an inert residual gas," J. Vacuum Sci.&Tech. B, 19, 2217 (2001).
[13] Kabashin, A. V., Meunier, M. "Laser-induced treatment of silicon in air and formation of Si/SiO_x photoluminescent nanostructured layers," Mat. Sci. Eng. B, 101, 60-64 (2003).
[14] Besner, S., Degorce, J.-Y., Kabashin, A. V., Meunier, M. "Influence of ambient medium on femtosecond laser processing of silicon," Appl. Surf. Sci., 247, 163-168 (2005).
[15] Kabashin, A. V., Meunier, M., "Femtosecond laser ablation in aqueous solutions: a novel method to synthesize non-toxic metal colloids with controllable size," J. Phys.: Conf. Series, 59, 354-357 (2007).
[16] Rioux, D. et al, "Silicon Nanoparticles Produced by Femtosecond Laser Ablation in Water as Novel Contamination-Free Photosensitizers," J. Biomed. Optics, 14, 021010 (2009).
[17] Blandin, P. et al., "Fs laser fragmentation from water-dispersed microcolloids: toward fast controllable growth of ultrapure Si-based nanomaterials for biological applications," J. Mater. Chem. B, 1, 2489-2495 (2013).
[18] Kabashin, A. V., Meunier, M. "Laser ablation-based synthesis of functionalized colloidal nanomaterials in biocompatible solutions," J. Photochemistry and Photobiology A, 182, 330-334 (2006).

[19] English, D. S.; Pell, L. E.; Yu, Z.; Barbara, P. F.; Korgel, B. A. "Size Tunable Visible Luminescence from Individual Organic Monolayer Stabilized Silicon Nanocrystal Quantum Dots," Nano Lett. 2, 681–685 (2002).
[20] Erogbogbo, F. et al, "Biocompatible Luminescent Silicon Quantum Dots for Imaging of Cancer Cells," ACS Nano, 2, 873–878 (2008).
[21] Timoshenko, V.Yu.; Kudryavtsev, A.A.; Osminkina, L.A.; Vorontzov, A.S.; Ryabchikov, Yu.V.; Belogorokhov, I.A.; Kovalev, D.; Kashkarov, P.K. "Silicon nanocrystals as photosensitizers of active oxygen for biomedical applications," JETP Lett., 83, 423-426 (2006).
[22] Xiao, L.; Gu, L.; Howell, S. B.; Sailor, M. J. "Porous silicon nanoparticles photosensitizers for singlet oxygen and their phototoxicity against cancer cells," ACS Nano, 5, 3651-3659 (2011).
[23] Lee, C.; Kim, H.; Hong, C.; Kim, M.; Hong, S. S.; Lee, D. H.; Lee, W. I. "Porous Silicon as an Agent for Cancer Thermotherapy Based on near-Infrared Light Irradiation," J. Mater. Chem., 18, 4790-4795 (2008).
[24] Sviridov, A. P.; Andreev, V. G.; Ivanova, E. M.; Osminkina, L. A.; Tamarov, K. P.; Timoshenko, V. Yu. "Porous Silicon Nanoparticles as Sensitizers for Ultrasonic Hyperthermia," Appl. Phys. Lett., 103, 193110 (2013).
[25] Maximova, K., Aristov, A. I., Sentis, M., Kabashin, A. V. "Size-controllable synthesis of bare gold nanoparticles by femtosecond laser fragmentation in water," Nanotechnology, 26, 065601 (2015).
[26] Theiss, W. "Optical properties of porous silicon," Surf. Sci. Rep. 29, 191-192 (1997).
[27] Timoshenko, V. Yu.; Dittrich, Th.; Lysenko, V.; Lisachenko, M. G.; Koch, F. "Free charge carriers in mesoporous silicon," Phys. Rev. B, 64, 085314 (2001).
[28] Maeda, H. "The Enhanced Permeability and Retention Effect in Tumor Vasculature: The Key Role of Tumor-Selective Macromolecular Drug Targeting," Adv. Enzyme Regul., 41, 189–207 (2001).